Journal of Power Sources 198 (2012) 359–367

Contents lists available at SciVerse ScienceDirect

Journal of Power Sources

journal homepage: www.elsevier.com/locate/jpowsour

A comparative study of equivalent circuit models for Li-ion batteries

Xiaosong Hu[a,b,*], Shengbo Li[a], Huei Peng[a]

[a] Department of Mechanical Engineering, The University of Michigan, Ann Arbor, MI 48109, USA
[b] Department of Mechanical Engineering, Beijing Institute of Technology, Beijing 100081, China

ARTICLE INFO

Article history:
Received 16 August 2011
Received in revised form 3 October 2011
Accepted 5 October 2011
Available online 12 October 2011

Keywords:
Equivalent circuit battery models
Battery management systems
Li-ion battery
Particle swarm optimization

ABSTRACT

This paper presents a comparative study of twelve equivalent circuit models for Li-ion batteries. These twelve models were selected from state-of-the-art lumped models reported in the literature. The test data used is obtained from a battery test system with a climate chamber. The test schedule is designed to measure key cell attributes under highly dynamical excitations. The datasets were collected from two types of Li-ion cells under three different temperatures. The multi-swarm particle swarm optimization algorithm is used to identify the optimal model parameters for the two types of Li-ion cells. The usefulness of these models is then studied through a comprehensive evaluation by examining model complexity, model accuracy, and robustness of the model by applying the model to datasets obtained from other cells of the same chemistry type.

1. Introduction

Hybrid electric vehicles (HEVs), plug-in hybrid electric vehicles (PHEVs) and battery electric vehicles (BEVs) are being actively developed and deployed to achieve significant fuel consumption and carbon emission reductions in many markets throughout the world. Traction battery packs are presently the performance and cost bottlenecks of these electrified vehicles. To ensure safe, reliable and efficient operations of the traction batteries under the most demanding and grueling driving conditions, an effective battery management system (BMS) must be used. A key function of the BMS is to monitor the conditions and states of the traction battery pack, such as State of Charge (SOC) and State-of-Health (SOH). Since these variables are not directly measurable by any sensors, they need to be inferred, commonly from model-based estimation algorithms [1–7]. Therefore, accurate battery models are of utmost importance. In addition to providing accurate estimations, it is important to strike a balance between model complexity and accuracy so that the models can be embedded in microprocessors and provide accurate results in real-time [8]. In other words, it is important to have models that are accurate enough, and not unnecessarily complicated.

Electrochemical models that aim to capture all key behaviors of battery cells [9–11] often can achieve high accuracy. They are suitable for understanding the distributed electrochemistry reactions in the electrodes and electrolyte [8]. However, they typically deploy partial differential equations with a large number of unknown parameters. The complexity often leads to significant requirement for memory and computation. In addition, they frequently run into over-fitting problems due to their significant number of parameters and the model robustness under extrapolation is typically poor—rendering their practical usefulness questionable. Hence, PDE-based electrochemical models are not desirable for actual battery management in electrified vehicles—if lumped battery models are accurate enough, they are likely to be the preferred choice.

Equivalent circuit battery models have been studied especially for the purpose of vehicle power management control and battery management system development. They are lumped models with relatively few number of parameters. For example, Plett [2] proposed several lumped models, including the simple, zero-hysteresis, one-state hysteresis, combined, and enhanced self correcting (ESC) models. In [2], test datasets of an HEV Li-polymer cell was used to compare these models. The resistance-capacitance (RC) network based equivalent circuit models were also widely studied, such as the first-order RC [12–14], second-order RC [15–17] and third-order RC models [18]. Dedicated elements depicting the battery hysteresis behavior were sometimes added to the RC models, such as the first-order RC model with hysteresis [19–21] and third-order RC model with hysteresis [22], etc. In the literature, there were few studies comparing these commonly used equivalent battery models. The goal of this paper is to systematically compare the practicality of these models, including model complexity, model accuracy under both training and validation data, and generalizability of these models to multiple cells. The last attribute is important because with improvement in battery chemistry, manufacturing process, cooling systems, and cell-to-cell balancing circuitry, it is likely the cell variations will continue to

* Corresponding author at: G041 Auto Lab., 1231 Beal Av., Ann Arbor, MI 48109-2133, USA. Tel.: +1 734 757 3563; fax: +1 734 757 3563.
E-mail address: huxiaos@umich.edu (X. Hu).

0378-7753/$ – see front matter © 2011 Elsevier B.V. All rights reserved.
doi:10.1016/j.jpowsour.2011.10.013

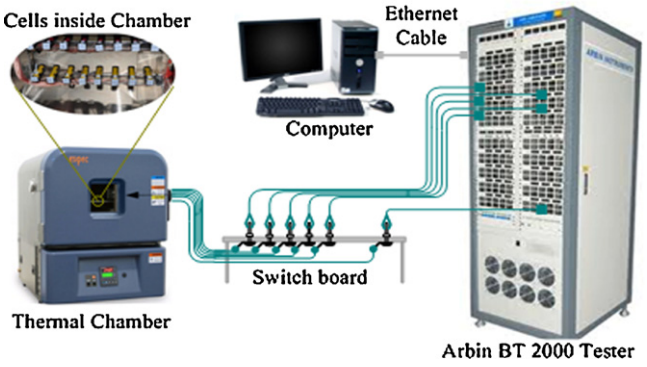

Fig. 1. Configuration of the battery test bench.

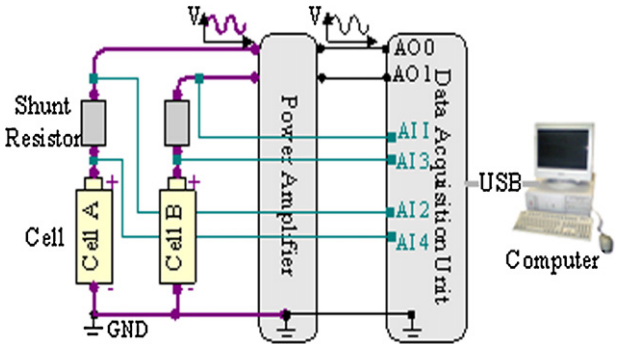

Fig. 2. Configuration of the ac impedance tester.

decrease, to such an extent that we may feel comfortable (or be driven economically) to measure and monitor the temperature and voltage of every few cells instead of each and every cell. To realize this vision, it is important to confirm that a model calibrated based on the measurements of one cell can be applied to predict the behavior of several adjacent cells placed under the same load and are operating under similar conditions such as environmental temperature.

In this paper, we study twelve commonly used lumped battery models. They are compared using multiple cell datasets we acquired under different temperatures for two types of Li-ion cells. The multi-swarm particle swarm optimization (MPSO) [23] is implemented to identify the optimal model parameters based on the training data from a single cell (arbitrarily selected from eight cells). Then, the usefulness of these models is compared by using validation test data obtained from eight cells of the same chemistry. This process was repeated for two types of Li-ion batteries.

The remainder of this paper is organized as follows. In Section 2, the experimental setup to acquire the data is described. In Section 3, the twelve equivalent circuit battery models are described. The MPSO-based model identification process is introduced in Section 4. The model comparison results are discussed in Section 5, followed by conclusions presented in Section 6.

2. Experimental setup

2.1. Battery testing systems

The experimental setup is shown in Fig. 1. It includes an Arbin BT2000 tester, a thermal chamber for environment control, a computer for user-machine interface and data storage, a switch board for cable connection, and the battery cells. During the charging/discharging, voltage, current, temperature of each cell is measured and recorded at 10 Hz.

An impedance measurement system (see Fig. 2) was also designed to record the battery impedance behavior at various excitation frequencies. It comprises a data acquisition unit for signal generation and data collection, a power amplifier for signal amplification, and two shunt resistors for current measurement. The measurement of impedance is obtained from sinusoidal excitations, in which both voltage and current in sinusoidal forms (with dc offset) are recorded and their complex quotient is computed as the cell impedance. To reduce measurement noise, a convolution-based method is adopted to identify the phase delay of impedance using the Parseval's Theorem for magnitude calculation [24]. Only two cells from each Li-ion cell types are tested and the sinusoidal input is modulated on top of a precisely generated dc offset to ensure we are not charging or discharging the cells during the test. The sampling time is input frequency dependent and can vary between 1/40 and 5 kHz.

Table 1
Main specifications of the LiNMC and $LiFePO_4$ cells.

Type	Nominal capacity (Ah)	Nominal voltage (V)	Upper cut-off voltage (V)	Lower cut-off voltage (V)
LiNMC	0.94	3.70	4.20	2.50
$LiFePO_4$	1.10	3.30	3.60	2.00

2.2. Battery test schedule

Two types of cylindrical Li-ion cells are selected for our tests. One is lithium nickel–manganese–cobalt oxide (LiNMC) UR14650P cells from Sanyo and the other is lithium iron phosphate ($LiFePO_4$) APR18650M1A cells from A123. Eight cells each were purchased on the open market. Their key specifications are shown in Table 1. These cells were placed in cell holders in the thermal chamber. They are independently tested using 16 channels of the battery tester. For the cells of the same chemistry, the same loading profile is applied.

The test schedules shown in Fig. 3 are designed to generate rich excitations for the two types of cells. Each experimental procedure takes about two weeks to finish. In each procedure, it begins with a characterization test at temperature $T = 10\,^{\circ}C$, followed by two identical tests conducted at $T = 35\,^{\circ}C$ and $T = 22\,^{\circ}C$. A static capacity test, a hybrid pulse test, a dc resistance test, a DST test and a FUDS test are consecutively conducted in each characterization test. The purpose of the static capacity test is to measure the cell capacity. The hybrid pulse test is a sequence of pulse cycles. Each pulse cycle is composed of the standard Hybrid Pulse Power Characterization (HPPC) profile and a self-designed discharging/charging

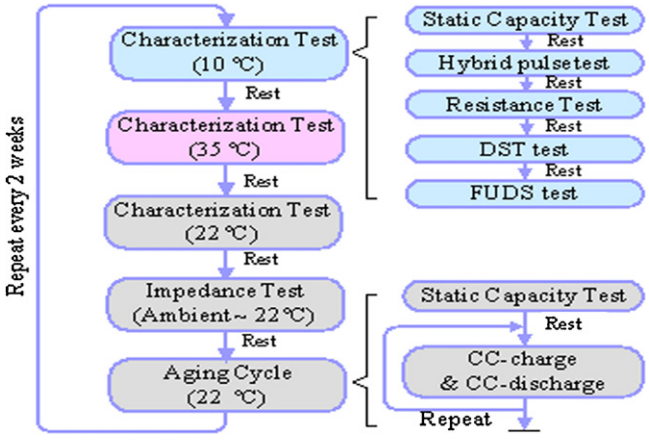

Fig. 3. Flow chart of the test schedule.

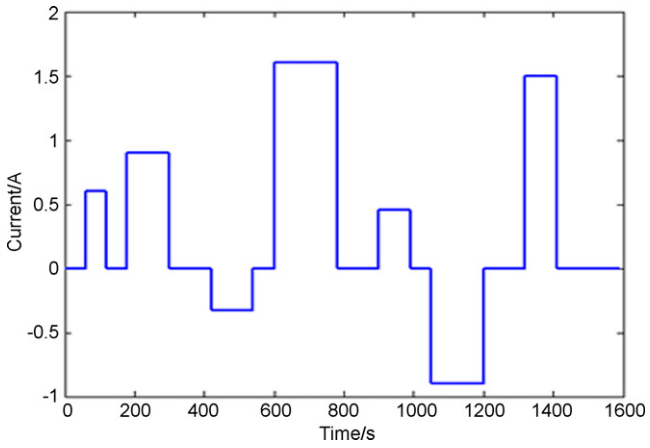

Fig. 4. Self-designed discharging/charging pulse profile for the LiNMC cells.

pulse profile. The self-designed profile is a combination of pulses with different amplitudes and durations. It serves two functions: to move the cell SOC, and to excite the cell dynamically. The self-designed pulse profile for LiNMC cells is shown in Fig. 4. That for $LiFePO_4$ cells is similar. The pulse amplitudes are merely enlarged to achieve the same current rates as those for LiNMC cells. The dc resistance test uses the standard testing program from Arbin to estimate the internal resistance. The Dynamic Stress Test (DST) and Federal Urban Dynamic Schedule (FUDS) tests excite the cells in driving cycle-based conditions. Between two adjacent test points in each characterization test the cells are charged or discharged to reach the desirable initial SOC values (around 90%) and rested to reach cell equilibrium. After these tests, the impedance test is conducted to collect data for battery impedance spectrum analysis. Then, the aging cycles are conducted at $T = 22\,^{\circ}C$. In each aging cycle, the cell is charged or discharged at a constant rate until the cut-off voltages.

2.3. Datasets for this work

The datasets collected in the three characterization tests for fresh cells in the first experimental procedure (before aging cycles) are used for the model identification and comparison in this paper. The hybrid pulse test datasets under three different temperatures for the reference cells (LiNMC cell in Channel 17, $LiFePO_4$ cell in Channel 25) are used as the training datasets. The DST and FUDS datasets for the reference cells serve as the model validation datasets. In addition, the hybrid pulse test, DST and FUDS datasets under three different temperatures for all the sixteen cells are used to assess the generalization of the optimized models to multiple cells. Since the SOC of the battery packs in electrified vehicles is not allowed to be less than a certain threshold (e.g., 20%) due to battery life consideration, the portion of the test data below 10% SOC in these datasets are not used in model comparison. The current, voltage and SOC of the reference LiNMC cell in the training dataset at $T = 22\,^{\circ}C$ are shown in Fig. 5. Note the dataset below 10% SOC was discarded. Similar pre-processing was done for the DST and FUDS datasets (see Figs. 6 and 7, a portion is showed to give more details).

3. Model structures

A total of twelve equivalent circuit battery models are selected from the literature and used in the study. These models were selected to form a comprehensive subset aiming to cover the majority of the lumped model templates studied in the past. The effects of battery SOC and current are covered explicitly in these models. In addition, the hysteresis observed during dynamic loading (mainly due to the Li-ion uneven distribution limited by

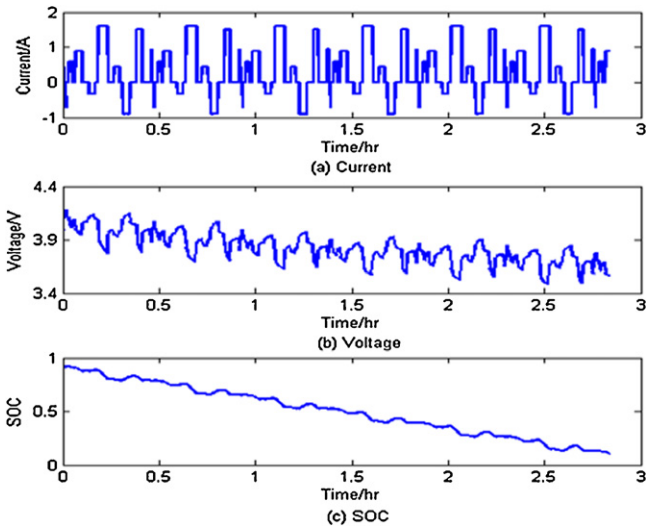

Fig. 5. Current, voltage and SOC of the reference LiNMC cell in the training dataset at 22 °C.

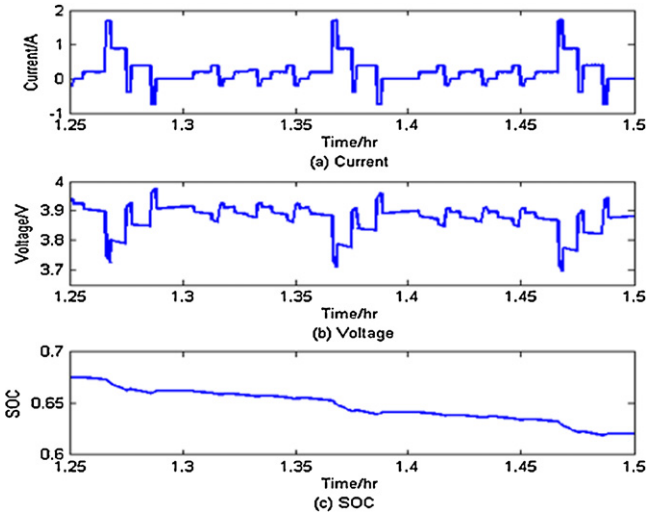

Fig. 6. Current, voltage and SOC of the reference LiNMC cell in a portion of the DST dataset at 22 °C.

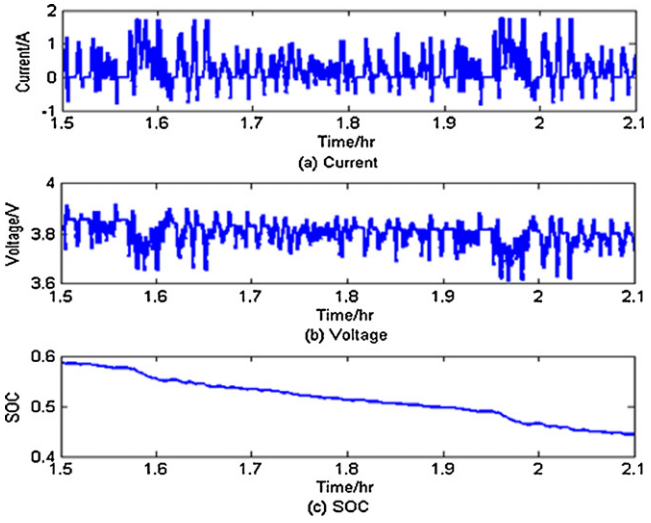

Fig. 7. Current, voltage and SOC of the reference LiNMC cell in a portion of the FUDS dataset at 22 °C.

Table 2
Twelve battery models.

Model	Model equations and description
(1) The combined model [2]	$V_k = K_0 - K_1/z_k - K_2 z_k + K_3 \ln(z_k) + K_4 \ln(1-z_k) - R_0 I_k$ where V_k, z_k and I_k are the battery terminal voltage, SOC and current, respectively; K_0, K_1, K_2, K_3 and K_4 are parameters for the dependence between open circuit voltage (OCV) and SOC; R_0 is the internal ohmic resistance which depends on the current direction. The optimization variable vector $\theta = [K_0, K_1, K_2, K_3, K_4, R_0^+, R_0^-]$.
(2) The simple model [2]	$V_k = \mathrm{OCV}(z_k) - R_0 I_k$ where $\mathrm{OCV}(z_k)$ represents the dependence between OCV and SOC in the form of a table. $\theta = [V_{oc,1}, \ldots, V_{oc,12}, R_0^+, R_0^-]$.
(3) The zero-state hysteresis model [2]	$V_k = \mathrm{OCV}(z_k) - R_0 I_k - s_k M$, $s_k = \begin{cases} 1, & I_k > \varepsilon, \\ -1, & I_k < -\varepsilon, \\ s_{k-1}, & \lvert I_K \rvert \le \varepsilon, \end{cases}$ where M is assumed to be a constant coefficient depicting the hysteresis level and ε is adequately small and positive. $\theta = [V_{oc,1}, \ldots, V_{oc,12}, R_0^+, R_0^-, M]$.
(4) The one-state hysteresis model [2]	$h_{k+1} = \exp(-\lvert \kappa I_k \Delta t \rvert) h_k + [1 - \exp(-\lvert \kappa I_k \Delta t \rvert)] H$ $V_k = \mathrm{OCV}(z_k) - R_0 I_k + h_k$ where h_k is the hysteresis voltage, κ is a decaying factor, Δt is the sampling time and H is the maximum amount of hysteresis voltage which is positive for charge and negative for discharge. $\theta = [V_{oc,1}, \ldots, V_{oc,12}, R_0^+, R_0^-, \kappa, H^+, H^-]$.
(5) The Enhanced Self-correcting (ESC) model (two-state low-pass filter) [2]	$\begin{bmatrix} f_{1,k+1} \\ f_{2,k+1} \\ h_{k+1} \end{bmatrix} = \begin{bmatrix} \alpha_1 & 0 & 0 \\ 0 & \alpha_2 & 0 \\ 0 & 0 & \exp(-\lvert \kappa I_k \Delta t \rvert) \end{bmatrix} \begin{bmatrix} f_{1,k} \\ f_{2,k} \\ h_k \end{bmatrix} + \begin{bmatrix} 1 & 0 \\ 1 & 0 \\ 0 & 1 - \exp(-\lvert \kappa I_k \Delta t \rvert) \end{bmatrix} \begin{bmatrix} I_k \\ H \end{bmatrix}$ $V_k = \mathrm{OCV}(z_k) - R_0 I_k + h_k + g_1 f_{1,k} + g_2 f_{2,k}$ where f_1 and f_2 are two states of a low-pass filter of the current; α_1 and α_2 are the diagonal elements of the state-transition matrix of the filter. g_1 and g_2 are the elements of the output matrix of the filter, and a zero-dc gain constraint is applied to them. $\theta = [V_{oc,1}, \ldots, V_{oc,12}, R_0^+, R_0^-, \kappa, H^+, H^-, \alpha_1, \alpha_2, g_1]$.
(6) The Enhanced Self-correcting (ESC) model (four-state low-pass filter) [2]	$\begin{bmatrix} f_{1,k+1} \\ f_{2,k+1} \\ f_{3,k+1} \\ f_{4,k+1} \\ h_{k+1} \end{bmatrix} = \begin{bmatrix} \alpha_1 & 0 & 0 & 0 & 0 \\ 0 & \alpha_2 & 0 & 0 & 0 \\ 0 & 0 & \alpha_3 & 0 & 0 \\ 0 & 0 & 0 & \alpha_4 & 0 \\ 0 & 0 & 0 & 0 & \exp(-\lvert \kappa I_k \Delta t \rvert) \end{bmatrix} \begin{bmatrix} f_{1,k} \\ f_{2,k} \\ f_{3,k} \\ f_{4,k} \\ h_k \end{bmatrix} + \begin{bmatrix} 1 & 0 \\ 1 & 0 \\ 1 & 0 \\ 1 & 0 \\ 0 & 1 - \exp(-\lvert \kappa I_k \Delta t \rvert) \end{bmatrix} \begin{bmatrix} I_k \\ H \end{bmatrix}$ $V_k = \mathrm{OCV}(z_k) - R_0 I_k + h_k + g_1 f_{1,k} + g_2 f_{2,k} + g_3 f_{3,k} + g_4 f_{4,k}$ where a four-state filter is used. $\theta = [V_{oc,1}, \ldots, V_{oc,12}, R_0^+, R_0^-, \kappa, H^+, H^-, \alpha_1, \alpha_2, \alpha_3, \alpha_4, g_1, g_2, g_3]$.
(7) The first-order RC model [12–14]	$U_{1,k+1} = \exp(-\Delta t/\tau_1) U_{1,k} + R_1 [1 - \exp(-\Delta t/\tau_1)] I_k$ $V_k = OCV(z_k) - R_0 I_k - U_{1,k}$ where U_1 and $\tau_1 = R_1 C_1$ are the voltage and time constant of the RC network. $\theta = [V_{oc,1}, \ldots, V_{oc,12}, R_0^+, R_0^-, R_1, \tau_1]$.
(8) The first-order RC model with one-state hysteresis [19–21]	$V_k = \mathrm{OCV}(z_k) - R_0 I_k - U_{1,k} + h_k$ where $\theta = [V_{oc,1}, \ldots, V_{oc,12}, R_0^+, R_0^-, \kappa, H^+, H^-, R_1, \tau_1]$.
(9) The second-order RC model [15–17]	$V_k = \mathrm{OCV}(z_k) - R_0 I_k - U_{1,k} - U_{2,k}$ where U_2 and $\tau_2 = R_2 C_2$ are the voltage and time constant of the second RC network. $\theta = [V_{oc,1}, \ldots, V_{oc,12}, R_0^+, R_0^-, R_1, \tau_1, R_2, \tau_2]$.
(10) The second-order RC model with one-state hysteresis	$V_k = \mathrm{OCV}(z_k) - R_0 I_k - U_{1,k} - U_{2,k} + h_k$ where $\theta = [V_{oc,1}, \ldots, V_{oc,12}, R_0^+, R_0^-, \kappa, H^+, H^-, R_1, \tau_1, R_2, \tau_2]$.
(11) The third-order RC model [18]	$V_k = \mathrm{OCV}(z_k) - R_0 I_k - U_{1,k} - U_{2,k} - U_{3,k}$ where U_3 and $\tau_3 = R_3 C_3$ are the voltage and time constant of the third RC network. $\theta = [V_{oc,1}, \ldots, V_{oc,12}, R_0^+, R_0^-, R_1, \tau_1, R_2, \tau_2, R_3, \tau_3]$.
(12) The third-order RC model with one-state hysteresis [22]	$V_k = \mathrm{OCV}(z_k) - R_0 I_k - U_{1,k} - U_{2,k} - U_{3,k} + h_k$ where $\theta = [V_{oc,1}, \ldots, V_{oc,12}, R_0^+, R_0^-, \kappa, H^+, H^-, R_1, \tau_1, R_2, \tau_2, R_3, \tau_3]$.

diffusion) is included explicitly. The effect of temperature however is not captured. The effect of which can be captured through temperature-dependent model parameters. These battery models are summarized in Table 2.

4. Identification of optimal model parameters

4.1. Optimization variables for the battery models

Out of the twelve models, except for model 1, the OCV is modeled as a function of SOC, and $V_{oc,j}, j = 1, 2, \ldots, 12$ is used to represent the jth optimization variable for describing OCV. When simulating the battery model, OCV is calculated by look-up table. The model variables to be optimized for all the twelve battery models are all summarized in Table 2. In this table, R_0^+ and R_0^- are internal ohmic resistances for the discharge and charge, respectively; H^+ and H^- denote the maximum hysteresis voltages for the discharge and charge, respectively. The bounds of the parameter vector to identify, θ_L and θ_U, were specified based on prior knowledge of the two types of Li-ion batteries. The bounds of the same parameters for different models are kept the same for fair comparison. For example, the upper bounds of R_0^+ in all the models were set to 0.2 Ω and 0.1 Ω for LiNMC and $LiFePO_4$ cells, respectively. It is important to note that $|\alpha_j| < 1$, $j = 1, \ldots, 4$ is imposed to ensure stability of the low-pass filters for the ESC models.

4.2. Optimization algorithm

To reduce the probability of trapped at a local minimum, the PSO-based global optimization approach was adopted. Compared to genetic algorithm, another global optimization method used for battery modeling [16,22], PSO has fewer parameters, has a more

Table 3
The numerical process of the multi-swarm particle swarm optimization (MPSO) method for battery model optimization.

Step 1: The bounds of the parameter vector, θ_L and θ_U, are assigned and the generation index *gen* is set to 0.
Step 2: Within the space bound, randomly generate an initial swarm (population) $\boldsymbol{P}_0$ which comprises N particles, i.e., $\boldsymbol{x}_1^0, \ldots, \boldsymbol{x}_N^0$. Each particle represents a candidate solution of the model parameters.
Step 3: Calculate $F(\boldsymbol{P}_0)$, and record personal bests of particles, i.e., $\boldsymbol{pbest}_1^0, \ldots, \boldsymbol{pbest}_N^0$, where $F(\cdot)$ is the objective function, half the sum of the squared voltage errors of the chosen model for the training dataset.
Step 4: If *gen* is less than the maximum generation, *Mgen*, perform the following steps (1)–(3).
(1) Split the swarm. Firstly sort the particles in a descending order according to their superiority levels determined by the objective function values. Then, the first particle is chosen as the local best of the first sub-swarm. $N_s - 1$ particles with the largest Euclidean distance from the local best are assigned to be the other members of the first sub-swarm. Repeat this selection procedure for the remaining particles until the remaining particles are less than N_s so as to establish all the sub-swarms.
(2) Evolve each particle in each sub-swarm by taking advantage of the velocity and position update equations of Krohling and Coelho's PSO. Note that the local best in each sub-swarm is updated with a probability of 85% to enhance the global search capability. The updated particle that violates the boundary constraint is adjusted to meet the boundary constraint.
(3) $gen = gen + 1$. Calculate $F(\cdot)$ for the updated swarm, and record updated personal best of particles according to their superiority levels, i.e., $\boldsymbol{pbest}_1^{gen}, \ldots, \boldsymbol{pbest}_N^{gen}$.
Step 5: If the generation index *gen* is equal to the maximum generation, *Mgen*, end the swarm evolution. Record the best particle in the final swarm and the best objective function value. The best particle is the optimized model parameter vector.

effective memory utilization, and is more efficient in maintaining the diversity of the search candidates [25]. A hybrid multi-swarm particle swarm optimization (HMPSO) algorithm for constrained optimization was developed to improve the global search capability of the standard PSO in [23]. In the new algorithm, the differential evolution (DE)-based mutation and swarm splitting concept are incorporated into the standard PSO. Since the DE-based mutation is too time-consuming for battery modeling on large datasets, MPSO was applied without DE. For MPSO, at each generation, the swarm is split into several sub-swarms and each sub-swarm evolves independently by taking advantage of the search equations of Krohling and Coelho's PSO [26], resulting in very effective diversity of the swarm. The general framework of MPSO for the battery model parameterization is shown in Table 3. The readers are referred to [23] for more details of the MPSO algorithm.

There are only three parameters to adjust for the MPSO algorithm, shown in Table 4. These values were found to generate good optimization results in our cases. A large value was assigned to the maximum generation variable, *Mgen* when identifying all the twelve models at the expense of slow computations. For each model, the optimization algorithm was individually executed on the training datasets under three different temperatures so that the temperature dependence can be added to the model.

5. Model optimization results

5.1. Model comparison using the training and validation datasets

The objective function for the model parameter optimization was defined for model accuracy, measured by the average root-mean-squared (RMS) error between the test datasets and the output from the optimized models. Experimental results from all three temperatures are used. However, the model parameters are allowed to change and be optimized for the three temperatures.

5.1.1. LiNMC battery reference cell

The maximum, minimum and average RMS errors of the twelve models optimized for the training datasets (hybrid pulse tests under three different temperatures) of the reference LiNMC cell are shown in Fig. 8. The model number is as shown in Table 2. It can be seen that the RC models are consistently more accurate than the first six models. In addition, adding one-state hysteresis to the RC models improves the average RMS error by about 7.9% compared to the first-order RC model without hysteresis. Adding RC networks can also improve the model accuracy however adding more complexity beyond 2RC network is not helpful.

Table 4
The three key parameters of the MPSO algorithm.

Parameter	*Mgen*	*N*	N_s
Value	10,000	60	8

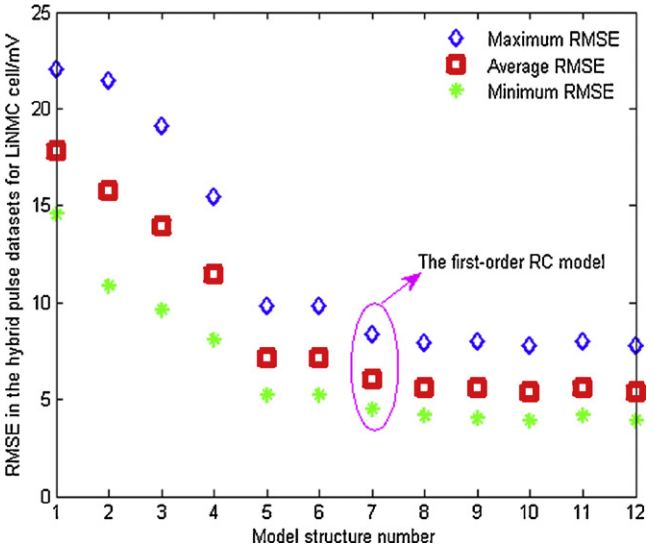

Fig. 8. Model training performance for the reference LiNMC cell.

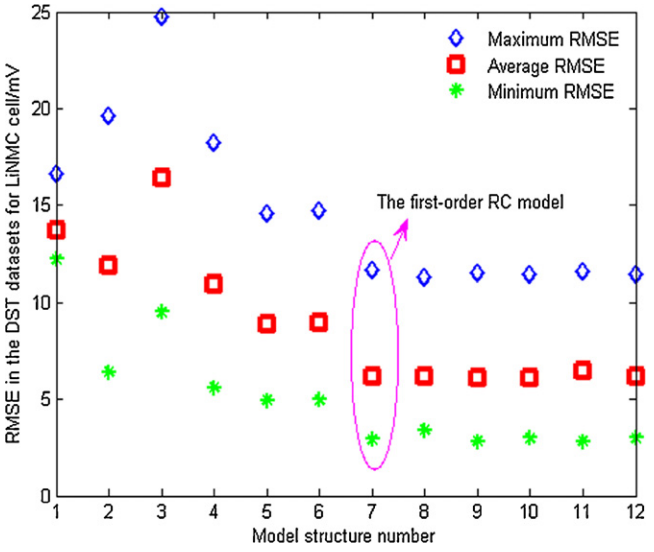

Fig. 9. Model validation performance for the reference LiNMC cell under the DST datasets.

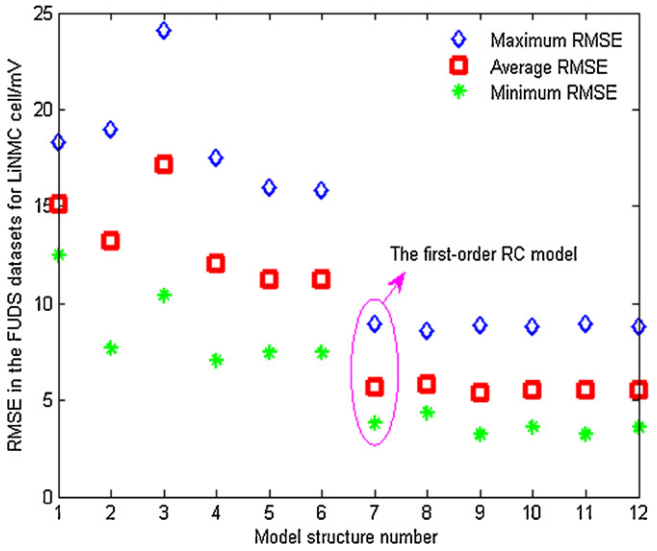

Fig. 10. Model validation performance for the reference LiNMC cell under the FUDS datasets.

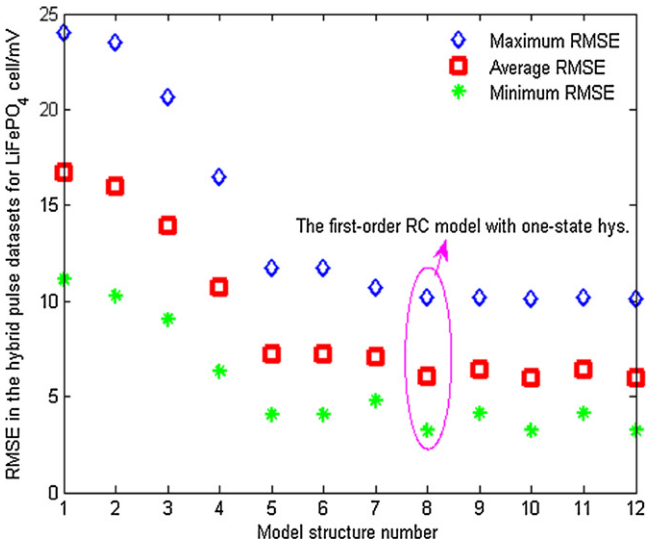

Fig. 12. Model training performance for the reference $LiFePO_4$ cell.

It is important to compare the model performance under unseen validation datasets, using which the model prediction capabilities are better evaluated. The RMS errors of the twelve models optimized for the hybrid pulse tests, but evaluated using the DST datasets (validation datasets) under three different temperatures are shown in Fig. 9. It can be seen that all twelve models have worse performance than under the training datasets. Among all twelve models, the zero-state hysteresis model has the worst validation result, indicating that its robustness might be a concern. Similar to the training results shown in Fig. 8, the RC models show consistently better performance compared to the first six models. The first-order RC model is almost as good as more complex models under the validation datasets-which seems to suggest it is a good choice balancing between model robustness and complexity.

The RMS errors of the twelve models under the FUDS datasets (another validation datasets) under three different temperatures are shown in Fig. 10. Since the FUDS test is a driving cycle-based test, the results are important. Again the first-order RC model stands out as the best model, achieving good prediction accuracy while using a simple model structure.

From the validations results above, we see that while more complicated models can achieve better accuracy under the training datasets, they seem to be more complicated than necessary, and their over-fitting characteristics does not help when the model is exposed to validation datasets that it has not seen before. Considering both model accuracy and model robustness, the first-order RC model is determined to be the best model for the LiNMC cell. The voltage responses of the first-order RC model and the reference LiNMC cell for one cycle in each dataset are shown in Fig. 11. The optimized battery model predicts cell voltage accurately.

While the numerical results clearly show the superior performance of the first-order RC model, one cannot but ask the following question: the low-pass filter in the ESC model seems to be conceptually similar to the function of a single RC network. So why is not the more complex model achieving better results under the training dataset? The first reason is numerical problem. Despite

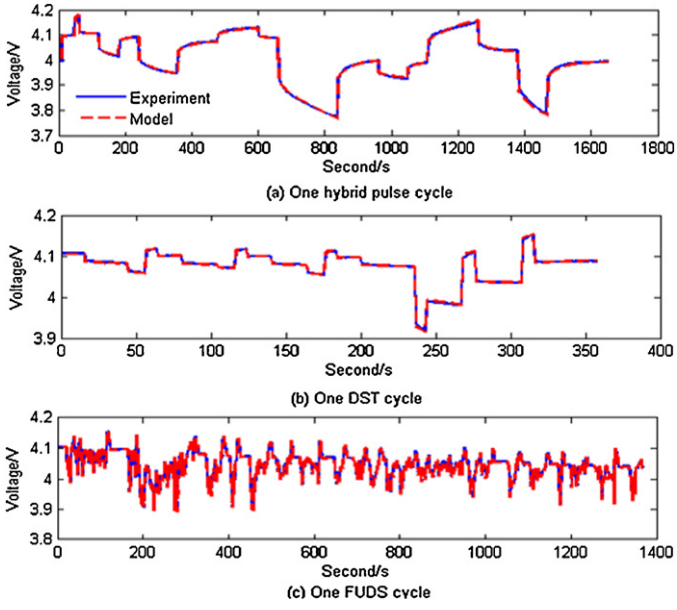

Fig. 11. Voltage responses of the first-order RC model and the reference LiNMC cell under 22 °C, (a) one hybrid pulse cycle (training); (b) one DST cycle (validation) and (c) one FUDS cycle (validation).

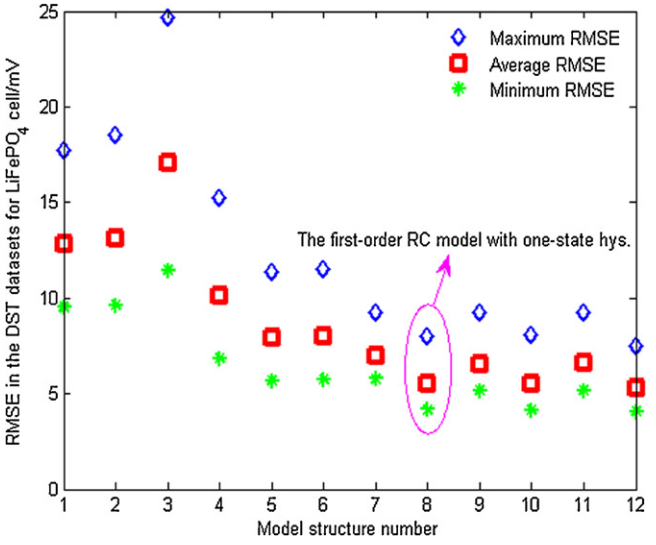

Fig. 13. Model validation performance for the reference $LiFePO_4$ cell under the DST datasets.

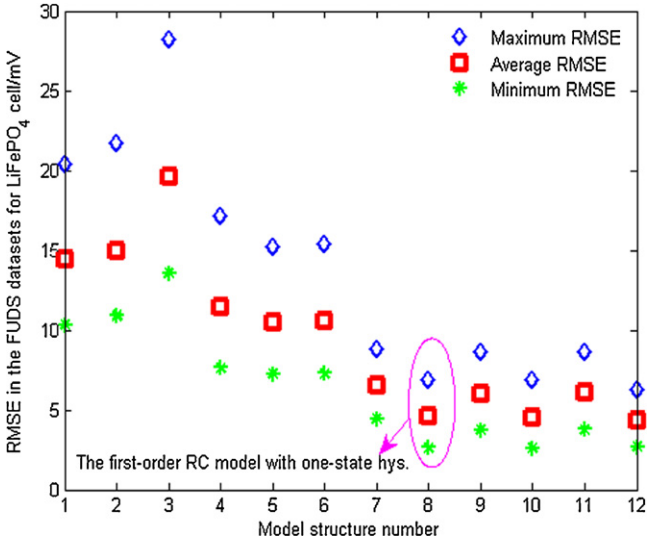

Fig. 14. Model validation performance for the reference $LiFePO_4$ cell under the FUDS datasets.

the fact we are using an optimization method with globally situated particle as search candidates, the solution is more prone to be trapped into local minima for more complicated models. Take the two-state low-pass filter in the ESC model as an example. Constraints $|\alpha_j| < 1$, $j = 1$, 2(stability) are too loose. From the optimization result of the second-order RC model with one-state hysteresis and $\alpha_1 \propto e^{-\Delta t/R_1C_1}$, $\alpha_2 \propto e^{-\Delta t/R_2C_2}$, we know that α_1, α_2 are in the intervals of [0.95, 1] and [0.98, 1]. (It is extremely difficult to know the two tight boundary constraints. Typically, we just know $|\alpha_j| < 1, j = 1, 2$ from our prior knowledge.) After tightening the constraints on α_1 and α_2, the optimization results can be improved. From numerical optimization viewpoint, the RC models are therefore better than the ESC models in terms of insensitiveness to boundary constraints and avoiding local minima. Although the optimization results can be improved by tightening the boundary constraints on α_1 and α_2, it is still worse than that of the second-order RC model with one-state hysteresis. This may be due to the

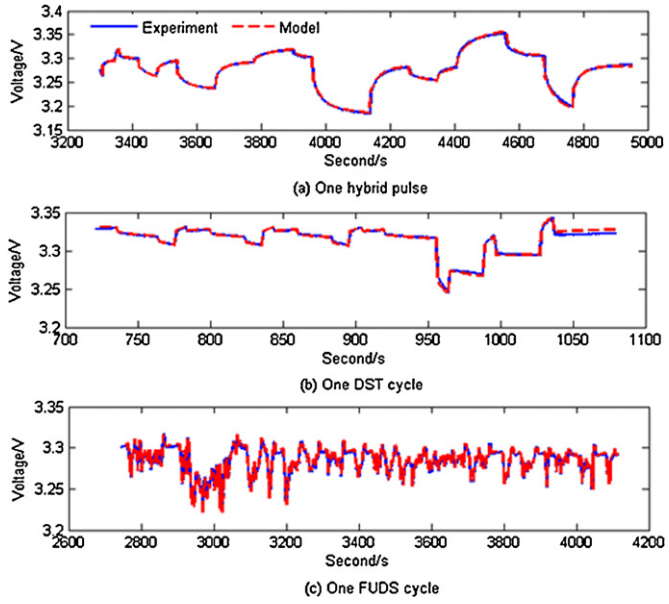

Fig. 15. The voltage responses of the first-order RC model with one-state hysteresis and the reference $LiFePO_4$ cell under 22 °C, (a) one hybrid pulse cycle (training); (b) one DST cycle (validation) and (c) one FUDS cycle (validation).

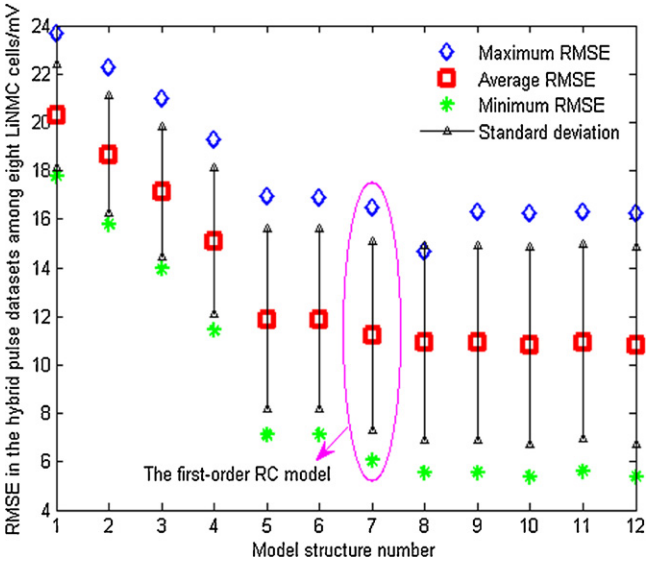

Fig. 16. Model generalization performance under the hybrid pulse test datasets for eight LiNMC cells.

zero-dc gain constraint for the ESC models which does not apply to the RC networks.

5.1.2. *$LiFePO_4$ battery reference cell*

The RMS errors of the twelve models optimized for the training datasets (the hybrid pulse power tests under three different temperatures) of the reference $LiFePO_4$ cell are shown in Fig. 12. The RC-network based models again show better performance compared to the first six models. It also seems that adding a one-state hysteresis to the RC-network models is helpful.

Again the optimized models are assessed using the DST and FUDS cycles to validate the robustness of the obtained models. The RMS errors of the twelve models using the DST and FUDS datasets under three different temperatures are shown in Figs. 13 and 14. It can be seen that the first-order RC model with one-state hysteresis is preferred for the $LiFePO_4$ cell, due to its balance between model complexity and accuracy. The voltage responses of the first-order RC model with one-state hysteresis and the reference cell for one cycle in each subtest in the characterization test under 22 °C are

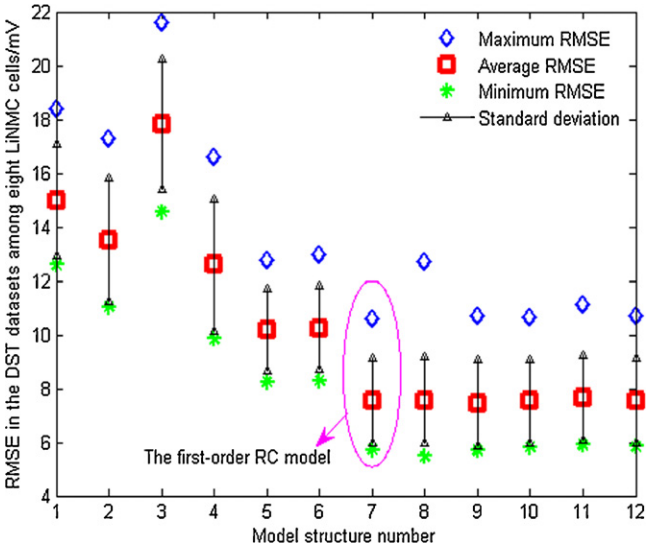

Fig. 17. Model generalization performance under the DST datasets for eight LiNMC cells.

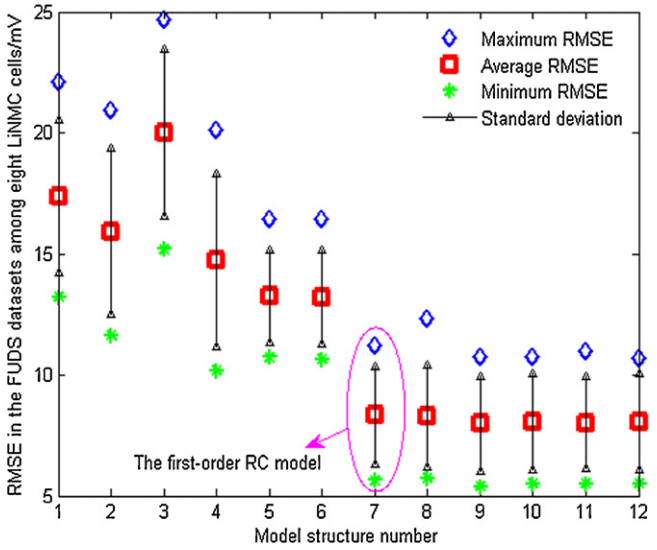

Fig. 18. Model generalization performance under the FUDS datasets for eight LiNMC cells.

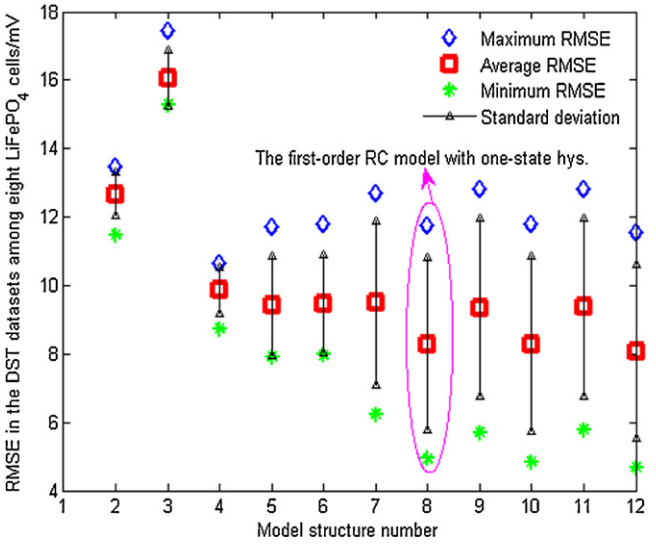

Fig. 20. Model generalization performance under the DST datasets for eight $LiFePO_4$ cells.

shown in Fig. 15. Again the model prediction output is accurate even under validation datasets.

5.2. Generalization to datasets from multiple cells

Traction battery pack in an electrified vehicle often consists of hundreds or even thousands of cells. Since safety is a major concern for Li-ion batteries, cell-level management and control are very important. For battery management, we can monitor and model each cell with its own sensors and models at the expense of significant hardware and computation cost. This arrangement is used in some early electrified vehicles because of the large cell-to-cell variations, caused by manufacturing variability, thermal gradient and other factors. With improved battery chemistry, manufacturing process controls, improved cooling systems, and cell-to-cell balancing circuitry, it is likely the cell variations will continue to decrease, to such an extent that we will feel comfortable to measure and monitor the temperature and voltage of every few cells instead of each and every cell. Under this envisioned future scenario, modeling each cell is unnecessary. Instead, it is possible we will generalize the model established and adapted for a single cell and use it to predict the behavior of several adjacent cells. Therefore, it is important to see which model structure works well when the model trained for one cell works on measured datasets from other cells. Here, the models obtained from the hybrid pulse testing datasets of the reference cells (LiNMC cell in Channel 17, $LiFePO_4$ cell in Channel 25) were used to predict the behavior of other cells of the same chemistry. The ability to "extrapolate to multiple cells" is measured by the maximum, minimum, and average RMS errors using the datasets from all eight cells of the same electrochemistry under the three different temperatures. The standard deviation of the RMS error is also calculated to demonstrate the spread of model error among eight cells.

5.2.1. LiNMC cell

The RMS errors of the twelve models under the hybrid pulse test datasets of all eight LiNMC cells are shown in Fig. 16, all of which are

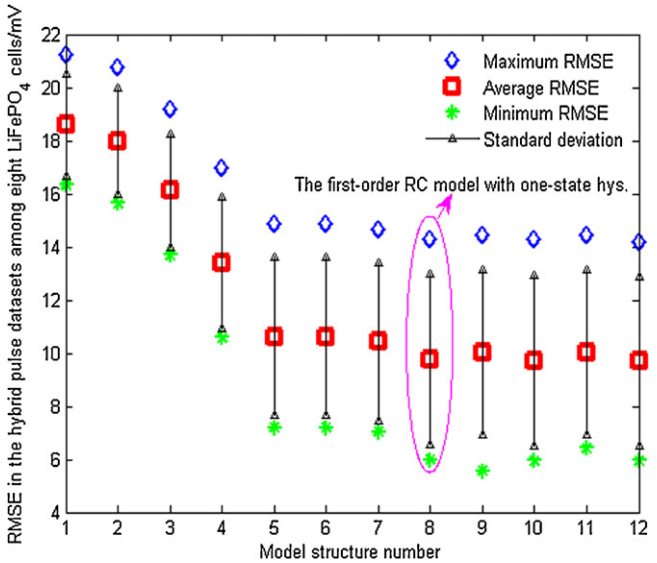

Fig. 19. Model generalization performance under the hybrid pulse test datasets for eight $LiFePO_4$ cells.

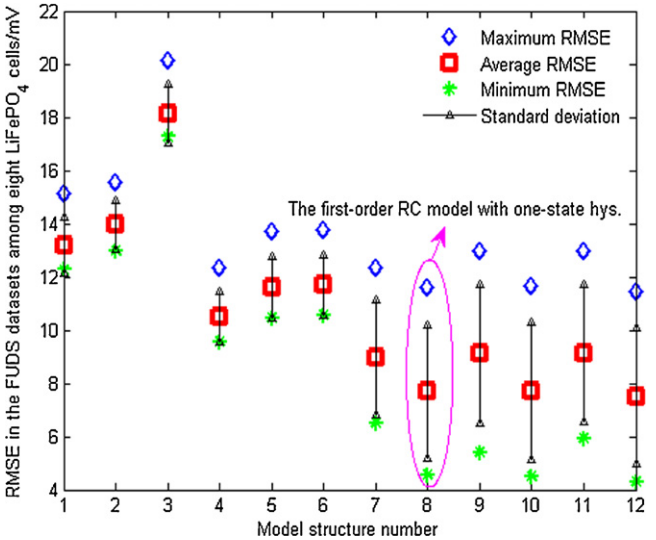

Fig. 21. Model generalization performance under the FUDS datasets for eight $LiFePO_4$ cells.

a little higher than those in Fig. 8, as one would expect. The average, min and max RMS errors again show similar trend. Adding RC networks or one-state hysteresis to the first-order RC model improves the model generalization capability a little. The maximum improvement on the average RMS error is approximately 2.8%. The RMS errors of the twelve models under the DST datasets of all eight LiNMC cells are shown in Fig. 17. Those under the FUDS datasets are shown in Fig. 18. It can be seen that the first-order RC model achieves good accuracy with minimum complexity.

5.2.2. $LiFePO_4$ cell

Similar to the LiNMC cells, results for the hybrid pulse test, DST and FUDS datasets of the eight $LiFePO_4$ cells are shown in Figs. 19–21, respectively. The first-order RC model with one-state hysteresis was again found to be the preferred choice.

6. Conclusions

A systematic comparative study of twelve lumped battery models is conducted. The MPSO algorithm is applied to conduct parameter optimizations. The model comparison is performed for two types of Li-ion cells, to assess their accuracies in both training and validation datasets, and generalization to multiple cells. Cells of the same chemistry seem to have very similar behavior, especially when they are new. It is thus possible to generalize the model established for a single cell to predict the behavior of several adjacent cells. The ability for a model to be generalized is thus important. Since complex models typically are more expensive and more susceptible to uncertainties, models that are accurate enough and yet simple are preferred. Comparison results indicate that the first-order RC model is preferred for LiNMC cells, while the first-order RC model with one-state hysteresis seems to be the best choice for $LiFePO_4$ cells. The developed cell voltage models can be used, e.g., in SOC estimation in battery management systems.

Acknowledgment

This work was supported by the Automotive Research Center (ARC), a U.S. Army center of excellence in modeling and simulation of ground vehicles.

References

[1] G.L. Plett, J. Power Sources 134 (2004) 252–261.
[2] G.L. Plett, J. Power Sources 134 (2004) 262–276.
[3] G.L. Plett, J. Power Sources 134 (2004) 277–292.
[4] G.L. Plett, J. Power Sources 161 (2006) 1356–1368.
[5] G.L. Plett, J. Power Sources 161 (2006) 1369–1384.
[6] I.S. Kim, J. Power Sources 163 (2006) 584–590.
[7] J.Y. Han, D.C. Kim, M. Sunwoo, J. Power Sources 188 (2009) 606–612.
[8] B. Pattipati, C. Sankavaram, K.R. Pattipati, IEEE Trans. Syst. Man Cybern. C: Appl. Rev. 41 (2011) 869–884, doi:10.1109/TSMCC.2010.2089979.
[9] C.Y. Wang, V. Srinivasan, J. Power Sources 110 (2002) 364–376.
[10] V.R. Subramanian, V. Boovaragavan, V. Ramadesigan, M. Arabandi, J. Electrochem. Soc. 156 (2009) A260–A271.
[11] A.P. Schmidt, M. Bitzer, A.W. Imre, L. Guzzella, J. Power Sources 195 (2010) 5071–5080.
[12] B.Y. Liaw, G. Nagasubramanian, R.G. Jungst, D.H. Doughty, Solid State Ionics 175 (2004) 835–839.
[13] M. Dubarry, N. Vuillaume, B.Y. Liaw, J. Power Sources 186 (2009) 500–507.
[14] Y.H. Chiang, W.Y. Sean, J.C. Ke, J. Power Sources 196 (2011) 3921–3932.
[15] M. Dubarry, B.Y. Liaw, J. Power Sources 174 (2007) 856–860.
[16] Y. Hu, S. Yurkovich, Y. Guezennec, B.J. Yurkovich, Control Eng. Pract. 17 (2009) 1190–1201.
[17] Y. Hu, S. Yurkovich, J. Power Sources 196 (2011) 2913–2923.
[18] D. Andre, M. Meiler, K. Steiner, H. Walz, T. Soczka-Guth, D.U. Sauer, J. Power Sources 196 (2011) 5349–5356.
[19] M. Verbrugge, E. Tate, J. Power Sources 126 (2004) 236–249.
[20] M. Verbrugge, B. Koch, J. Electrochem. Soc. 153 (2006) A187–A201.
[21] M. Verbrugge, J. Appl. Electrochem. 37 (2007) 605–616.
[22] Y. Hu, S. Yurkovich, Y. Guezennec, B.J. Yurkovich, J. Power Sources 196 (2011) 449–457.
[23] Y. Wang, Z.X. Cai, Front. Comput. Sci. Chin. 3 (2009) 38–52.
[24] J. Proakis, D. Manolakis, Digital Signal Processing: Principle, Algorithm, and Applications, third ed., Prentice-Hall, New Jersey, 1996.
[25] Y.D. Valle, G.K. Venayagamoorthy, S. Mohagheghi, J.C. Hernandez, R.G. Harley, IEEE Trans. Evol. Comput. 12 (2008) 171–195.
[26] R.A. Krohling, L.S. Coelho, IEEE Trans. Syst. Man Cybern. B: Cybern. 36 (2006) 1407–1416.